Self-phase-modulation of surface plasmon polaritons

Israel De Leon,[1,*] J. E. Sipe,[2] and Robert W. Boyd[1,3]
[1]*Department of Physics, University of Ottawa, 150 Louis Pasteur St., Ottawa, Canada K1N6N5*
[2]*Department of Physics, University of Toronto, 60 St. George St., Toronto, Canada M5S1A7*
[3]*The Institute of Optics, University of Rochester, Rochester, New York 14627, USA*
(Received 25 November 2013; published 31 January 2014)

We present an approach for calculating the nonlinear propagation of surface plasmon polaritons in one-dimensional planar waveguides consisting of a metal slab or a semi-infinite metal bounded by linear dielectrics, starting with an assumed third-order nonlinearity that characterizes the nonlinear response of the metal. With this approach we model the self-phase-modulation of surface plasmon polaritons. Expressions relating the complex nonlinear parameter of these surface waves with the third-order nonlinear susceptibility of the metal are provided. We present and discuss results pertaining to the self-phase-modulation of the symmetric and antisymmetric surface plasmon polaritons supported by a thin gold slab in vacuum and of the surface plasmon polariton supported by the single gold-vacuum interface.

DOI: 10.1103/PhysRevA.89.013855 PACS number(s): 42.65.Tg, 73.20.Mf, 42.65.Hw, 42.65.Wi

I. INTRODUCTION

For decades, nonlinear optical effects have proved useful for many different applications, such as nonlinear microscopy [1], ultrafast laser systems [2], optical frequency conversion [3], and all-optical switching [4]. Recently, there has been much interest in studying these phenomena at the nanoscale, particularly in *plasmonic* structures [5]. Such structures typically incorporate nanoscopic metallic features that enable enhanced nonlinear effects mediated by surface plasmon polaritions (SPPs), which are collective charge oscillations coupled to photons at the surface of metals [6]. For extended metal surfaces, these collective excitations take the form of transverse-magnetic (TM) polarized optical surface waves that propagate along the metal's surface. Because of their capacity to concentrate intense fields over subwavelength scales, SPPs can enhance nonlinear optical processes in metallic nanoparticles as well as at extended metal surfaces [7,8]. As a result, numerous theoretical and experimental works have studied nonlinear effects in different plasmonic structures such as flat and patterned metallic surfaces [9–12], layered metalodielectric structures [13–15], and metallic nanoparticles [16–19].

The nonlinear response of SPPs propagating along different types of plasmonic waveguides has been theoretically investigated by several groups [20–27]. In most of these studies it is assumed that the nonlinearity results from a Kerr-type nonlinear dielectric bounding the metal, while the metal is taken as a linear medium. However, SPPs are intrinsically nonlinear (even in the absence of a nonlinear dielectric) as they exist on structures composed of metallic media, which exhibit strong and ultrafast third-order nonlinear response at optical wavelengths [28,29]. Thus it is important to develop methods to study and design nonlinear plasmonic waveguides based on this intrinsic nonlinear response.

In this work we present an approach for calculating the intrinsic nonlinear propagation of SPPs supported by two typical plasmonic waveguides: a metallic slab and a semi-infinite metal bounded by linear dielectrics. In particular, we use this approach to model the phenomenon of self-phase-modulation, whereby the complex propagation constant of the SPP is modified by the SPP itself via the third-order nonlinearity of the metal. We derive an expression for the complex nonlinear parameter that characterizes the self-phase-modulation in terms of the structural properties of the waveguide, and use it to construct a differential equation that describes the evolution of the SPP's complex amplitude. Solving this differential equation provides us with a self-consistent way to estimate the nonlinear phase and nonlinear loss experienced by the SPP upon propagation. We employ our approach to estimate the maximum nonlinear phase shift acquired by the various SPP modes supported by two structures of interest, using gold (Au) as the metal and vacuum playing the role of the dielectric. Finally, we compare the results of our method with recent experimental results and present a discussion around it.

II. STRUCTURES INVESTIGATED

The structures investigated are shown in Figs. 1(a) and 1(b). The first structure consist of a metal slab that occupies the region $0 > z > -d$ and is bounded by dielectrics. The relative permittivity of the metal is denoted by ε_3, and those of the dielectrics above ($z > 0$) and below ($z < -d$) the slab are denoted by ε_1 and ε_2, respectively. The second structure is a single metal-dielectric interface, which corresponds to the case of a slab with infinite thickness. We shall refer to the metal, top dielectric, and bottom dielectric as media 3, 1, and 2, respectively. We consider linear dielectrics with $\mathrm{Re}\varepsilon_1, \mathrm{Re}\varepsilon_2 > 0$, and a metal with $\mathrm{Re}\varepsilon_3 < 0$, such that SPPs are supported by the system. Furthermore, we consider a metal whose optical nonlinearity is characterized by a third-order nonlinear susceptibility, $\chi^{(3)}$.

When the thickness of the slab is large, the structure supports a bound SPP at each metal-dielectric interface. However, when this thickness is comparable to the optical penetration depth into the metal, the SPPs at each interface couple giving rise to different SPP modes. Two of these new modes are bound [30,31]. For the case when $\varepsilon_1 \neq \varepsilon_2$, the z component of the electric fields associated with these bound

*ideleon@uottawa.ca

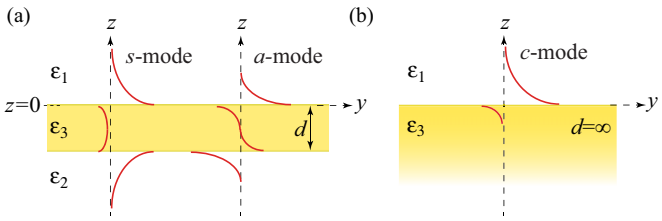

FIG. 1. (Color online) Structures investigated: (a) metal slab of thickness d bound by linear dielectrics; (b) single metal-dielectric interface corresponding to case in (a) where $d = \infty$. The z component of the fields (real part) associated with the various SPP modes supported are outlined.

modes exhibit a quasisymmetric and a quasiantisymmetric distribution along the z direction. On the other hand, for $\varepsilon_1 = \varepsilon_2$, these modes have a true symmetric and antisymmetric transverse distribution, as sketched in Fig. 1(a). We shall refer to the symmetric (or quasisymmetric) mode as the s mode and to the antisymmetric (or quasiantisymmetric) mode as the a mode. In general, the a mode has a significant part of the field in the metal; hence it exhibits a very large propagation loss; on the other hand, the s mode has most of the field in the bounding dielectrics, which leads to a relatively small propagation loss. For the infinitely thick slab, the structure supports only one mode; i.e., the *conventional* single-interface SPP mode. We shall refer to this mode as the c mode. The z component of the SPP transverse electric-field distribution is outlined in Fig. 1(b). For this, the portion of the field in the metal, and hence the propagation loss of the mode, is in between that of the a mode and the s mode.

III. THEORETICAL MODEL

Throughout the text, all the fields are assumed to have the form $\boldsymbol{F}(\boldsymbol{r},t) = \boldsymbol{F}(\boldsymbol{r})\exp(-i\omega t) + \text{c.c.}$, where c.c. denotes the complex conjugate and the position vector is defined in the (y,z) plane; i.e., $\boldsymbol{r} = z\hat{\boldsymbol{z}} + y\hat{\boldsymbol{y}}$. Furthermore, it will be useful for our analysis to write the SPP electric field as

$$\boldsymbol{E}(\boldsymbol{r}) = f(y)\mathbf{e}(z)e^{i\kappa'_m y}. \tag{1}$$

Here and below, $m = \{s,a,c\}$ denote the various SPP modes, $f(y)$ is the field envelope function, which describes the evolution of the field's amplitude as the SPP propagates in the y direction, $\mathbf{e}(z)$ is the transverse electric-field distribution, and $\kappa'_m = \text{Re}\kappa_m$, with κ_m being the SPP propagation constant.

For linear propagation, $f(y)$ is a real function that satisfies the homogeneous differential equation,

$$\frac{df(y)}{dy} = -\kappa''_m f(y), \tag{2}$$

where $\kappa''_m = \text{Im}\kappa_m$. The solution of this equation describes the typical exponential decay of the SPP field as the wave propagates, which results from the linear optical absorption in the metal. This description is no longer valid for nonlinear propagation, as the SPP experiences an additional nonlinear phase and loss. Indeed, for self-phase-modulation, the nonlinear phase and loss acquired by the SPP render $f(y)$ a complex function that depends on the intensity of the SPP itself. The purpose of the present analysis is to formulate a differential equation describing the behavior of $f(y)$ accounting for the process of self-phase-modulation.

The remainder of this section is divided in four sections that explain our theoretical approach. In Sec. III A we obtain expressions for the linear SPP fields of the slab waveguide, as they will be used later for the nonlinear analysis. In Sec. III B we employ a Green-function formalism to formulate a differential equation for $f(y)$ in the slab waveguide, allowing the presence of an arbitrary nonlinear polarization field in the metal. In Sec. III C we use the results of previous sections to model the self-phase-modulation of SPPs by letting the nonlinear polarization in the metal be generated by the SPP field, and in Sec. III D we extend these results to the single-interface waveguide by taking the limit where the thickness of the metal slab is infinite.

A. Linear response

We treat the nonlinear problem as a perturbative approach to the linear solution, assuming that the nonlinearity modifies the form of $f(y)$ but not the form of $\mathbf{e}(z)$. Thus we start our analysis by obtaining the transverse field distribution, $\mathbf{e}(z)$, in the linear regime for the structure shown in Fig. 1(a). We consider a TM-polarized plane wave in medium 1 that propagates downwards in the (z,y) plane and impinges onto the structure at $z = 0$. After a simple reflection and transmission analysis, one finds electric fields of the form

$$\begin{aligned}
\boldsymbol{E}_1(\boldsymbol{r}) &= E_0[\hat{\boldsymbol{p}}_{1-}e^{-iw_1 z} + \hat{\boldsymbol{p}}_{1+}R_{12}e^{iw_1 z}]e^{i\kappa y},\\
\boldsymbol{E}_3(\boldsymbol{r}) &= E_0 T_{12}t_{32}^{-1}[\hat{\boldsymbol{p}}_{3-}e^{-iw_3(z+d)} + \hat{\boldsymbol{p}}_{3+}r_{32}e^{iw_3(z+d)}]e^{i\kappa y},\\
\boldsymbol{E}_2(\boldsymbol{r}) &= E_0 T_{12}[\hat{\boldsymbol{p}}_{2-}e^{-iw_2(z+d)}]e^{i\kappa y}
\end{aligned} \tag{3}$$

for media 1, 3, and 2, respectively. The different quantities in (3) are defined as follows: E_0 is the electric-field strength of the incident plane wave, κ is the wave-vector component in the plane of the surface, and the wave-vector component perpendicular to the surface is $\pm w_i$, where $w_i = \sqrt{\tilde{\omega}^2\varepsilon_i - \kappa^2}$, with $\tilde{\omega} = \omega/c$ being the wave number in free space. To completely define w_i, we take the sign of the square root that makes $\text{Im}w_i \geqslant 0$, and if $\text{Im}w_i = 0$ then we take the sign that makes $\text{Re}w_i \geqslant 0$. The unit TM-polarization vectors, $\hat{\boldsymbol{p}}_{i\pm}$, denote the polarization of the electric fields in the different media and are given by

$$\hat{\boldsymbol{p}}_{i\pm} = \frac{\kappa\hat{\boldsymbol{z}} \mp w_i\hat{\boldsymbol{y}}}{\tilde{\omega}\sqrt{\varepsilon_i}}, \tag{4}$$

where the subindex $i+$ $(i-)$ indicates that the polarization vector is associated with radiation in medium $i = \{1,2,3\}$ propagating in the positive (negative) z direction. The Fresnel reflection (r_{ij}) and transmission (t_{ij}) coefficients of the individual metal-dielectric interfaces for TM polarization are

$$r_{ij} = \frac{w_i\varepsilon_j - w_j\varepsilon_i}{w_i\varepsilon_j + w_j\varepsilon_i}, \quad t_{ij} = \frac{2\sqrt{\varepsilon_i}\sqrt{\varepsilon_j}w_i}{w_i\varepsilon_j + w_j\varepsilon_i}, \tag{5}$$

and the reflection (R_{12}) and transmission (T_{12}) coefficients of the slab (i.e., the response coefficients) are given by the usual

expressions

$$R_{12} = p(\kappa)(r_{32}e^{2iw_3d} + r_{13}),$$
$$T_{12} = p(\kappa)t_{13}t_{32}e^{iw_3d}, \tag{6}$$

with

$$p(\kappa) = (1 - r_{31}r_{32}e^{2iw_3d})^{-1}. \tag{7}$$

The fields in (3) are typically used when one actually has an incident wave making an angle φ from the normal in medium 1, in which case $\kappa = \tilde{\omega}\sqrt{\varepsilon_1}\sin\varphi$. Nonetheless, these fields are solutions of the Maxwell equations for any κ, including $\kappa > \tilde{\omega}\sqrt{\varepsilon_1}$ (corresponding to values of φ beyond the critical angle) for which SPPs are found. With this in mind, and noting that the s and a modes have propagation constants κ_m associated with the poles of $p(\kappa)$, we approximate (6) for κ close to κ_m by replacing $p(\kappa)$ with the contribution of its pole at κ_m, yielding

$$R_{12}^m \approx \frac{\rho_{12}}{\kappa - \kappa_m} \quad \text{with} \quad \rho_{12} = \varrho_m\left(r_{32}^m e^{2iw_3^m d} + r_{13}^m\right), \tag{8a}$$

$$T_{12}^m \approx \frac{\tau_{12}}{\kappa - \kappa_m} \quad \text{with} \quad \tau_{12} = \varrho_m t_{13}^m t_{32}^m e^{iw_3^m d}. \tag{8b}$$

In these expressions, ϱ_m is a complex-valued quantity that can be calculated using standard pole analysis techniques, as detailed in Appendix A. Here and below, we use the superscript m in various functions of κ to indicate that κ has been replaced by κ_m.

At the SPP excitation, the field in medium 1 is evanescent in the z direction; i.e., $\boldsymbol{E}_1(z) \propto \hat{\boldsymbol{p}}_{1+}^m \exp(iw_1^m z)$. In this situation, the term associated with the incident wave in expression (3) must vanish, otherwise it would diverge as $z \to \infty$. This is possible only if E_0 vanishes as $\kappa \to \kappa_m$. Thus, to obtain the electric-field distribution of the various SPP modes of the slab, we use (8) in (3) and set $E_0 \propto (\kappa - \kappa_m)$, while letting $\kappa \to \kappa_m$. This yields

$$\begin{aligned}
\boldsymbol{E}_1(\boldsymbol{r}) &\propto \hat{\boldsymbol{p}}_{1+}^m \rho_{12} e^{iw_1^m z} e^{i\kappa_m y},\\
\boldsymbol{E}_3(\boldsymbol{r}) &\propto \frac{\tau_{12}}{t_{32}^m}\left[\hat{\boldsymbol{p}}_{3-}^m e^{-iw_3^m(z+d)} + \hat{\boldsymbol{p}}_{3+}^m r_{32}^m e^{iw_3^m(z+d)}\right] e^{i\kappa_m y},\\
\boldsymbol{E}_2(\boldsymbol{r}) &\propto \hat{\boldsymbol{p}}_{2-}^m \tau_{12} e^{-iw_2^m(z+d)} e^{i\kappa_m y}.
\end{aligned} \tag{9}$$

This expression can be cast in the form of (1) by using the field envelope function, $f(y)$, as the proportionality constant (with units of V/m) and writing the transverse field, $\mathbf{e}(z)$, in the different regions as

$$\begin{aligned}
\mathbf{e}_1(z) &= \hat{\boldsymbol{p}}_{1+}^m e^{iw_1^m z},\\
\mathbf{e}_3(z) &= \frac{\tau_{12}}{\rho_{12}t_{32}^m}\left[\hat{\boldsymbol{p}}_{3-}^m e^{-iw_3^m(z+d)} + \hat{\boldsymbol{p}}_{3+}^m r_{32}^m e^{iw_3^m(z+d)}\right],\\
\mathbf{e}_2(z) &= \frac{\tau_{12}}{\rho_{12}}\hat{\boldsymbol{p}}_{2-}^m e^{-iw_2^m(z+d)}.
\end{aligned} \tag{10}$$

Of course, this agrees with the result of the more common strategy for finding the SPP field [31], based on applying the conditions the fields satisfy on crossing the interfaces at $z = 0$ and $z = -d$.

The power per unit length (along the x direction) carried by the SPP, $s(y)$, is obtained from the time-averaged Poynting vector as the power flow along the y direction; i.e., $s(y) = 2\,\mathrm{Re}\int_{-\infty}^{\infty}(\boldsymbol{E}\times\boldsymbol{H}^*)\cdot\hat{\boldsymbol{y}}\,dz$. Here, $\boldsymbol{H} = (i\omega\mu_0)^{-1}\nabla\times\boldsymbol{E}$ is the magnetic field with μ_0 being the vacuum permeability. Using this expression together with (1) and (10) one obtains

$$s(y) = \mathcal{K}_m|f(y)|^2, \tag{11}$$

where

$$\mathcal{K}_m = \frac{\mathrm{Re}\kappa_m}{\omega\mu_0}\left[\frac{\mathrm{Re}\varepsilon_1^{-1}|\varepsilon_1|}{\mathrm{Im}w_1^m} + \left|\frac{\tau_{12}}{\rho_{12}}\right|^2\frac{\mathrm{Re}\varepsilon_2^{-1}|\varepsilon_2|}{\mathrm{Im}w_2^m} + \left|\frac{r_{31}^m}{t_{31}^m}\right|^2\left(\frac{\sigma_1\mathrm{Re}\varepsilon_3^{-1}|\varepsilon_3|}{\mathrm{Im}w_3^m} + \frac{\sigma_2\mathrm{Re}\varepsilon_3^{-1}|\varepsilon_3|}{\mathrm{Re}w_3^m}\right)\right], \tag{12}$$

with $\sigma_1 = (|r_{32}^m|^2e^{-2d\,\mathrm{Im}w_3^m} + 1)(1 - e^{-2d\,\mathrm{Im}w_3^m})$ and $\sigma_2 = \mathrm{Re}i(1 - e^{-2id\,\mathrm{Re}w_3^m})/(r_{31}^m)$. Equations (11) and (12) will be useful for our nonlinear analysis in the following sections. Note that these equations hold in the nonlinear regime because we assume that linear transverse fields in (10) retain their form in the presence of nonlinearities.

B. Nonlinear response

We shall now proceed to study the nonlinear response of SPPs supported by the structure shown in Fig. 1(a).

As a preliminary, consider first the linear response of the slab structure to a specified source polarization located in the metal layer and having the form of a two-dimensional sheet extended over the (x,y) plane at $z = z_0$. This polarization distribution is defined mathematically as $\tilde{\boldsymbol{\wp}}\delta(z - z_0)\exp(i\kappa y)$ with the vector $\tilde{\boldsymbol{\wp}}$ lying in the (y,z) plane and $-d < z_0 < 0$. In turn, the electric field generated by such a polarization sheet has the form $\tilde{\boldsymbol{E}}(\kappa;z,z_0)\exp(i\kappa y)$. Generated fields in planar structures involving surfaces, such as the one studied here, can be obtained using a Green-function formalism detailed earlier [32]. Here, we employ this method to obtain the coefficient $\tilde{\boldsymbol{E}}(\kappa;z,z_0)$; we state only the final solution and refer the reader to the literature for details [in particular, refer to Sec. 4 of Ref. [32] and to the discussion around Eqs. (4.8) to (4.21)]. For the metal slab geometry one obtains

$$\tilde{\boldsymbol{E}}(\kappa;z,z_0) = \frac{i\tilde{\omega}^2 p(\kappa)}{2\varepsilon_0 w_3}\tilde{\boldsymbol{\wp}}\cdot\mathsf{q}(z,z_0) - \frac{1}{\varepsilon_0\varepsilon_3}\delta(z - z_0)\tilde{\boldsymbol{\wp}}\cdot\hat{\mathbf{z}}\hat{\mathbf{z}}, \tag{13}$$

where the first term on the right-hand side is related to the part of the fields radiated by the polarization sheet and the second term is a local contribution of the polarization sheet. In this expression, ε_0 is the vacuum permittivity and $\mathsf{q}(z,z_0)$ is a tensor given by

$$\begin{aligned}
\mathsf{q}(z,z_0) = {}& \boldsymbol{u}(z_0)\hat{\boldsymbol{p}}_{1+}t_{31}e^{iw_1z}\theta(z)\\
&+ \boldsymbol{v}(z_0)\hat{\boldsymbol{p}}_{2-}t_{32}e^{-iw_2(z+d)}\theta(-z-d)\\
&+ \boldsymbol{u}(z_0)[\hat{\boldsymbol{p}}_{3+}e^{iw_3z} + \hat{\boldsymbol{p}}_{3-}r_{31}e^{-iw_3z}]\theta(z-z_0)\theta(-z)\\
&+ \boldsymbol{v}(z_0)[\hat{\boldsymbol{p}}_{3+}r_{32}e^{iw_3(z+d)} + \hat{\boldsymbol{p}}_{3-}e^{-iw_3(z+d)}]\\
&\times\theta(z_0-z)\theta(z+d),
\end{aligned} \tag{14}$$

where $\theta(z)$ is the Heaviside function, which is defined as $\theta(z) = 1$ for $z > 0$ and $\theta(z) = 0$ for $z < 0$, and the functions

$\boldsymbol{u}(z)$ and $\boldsymbol{v}(z)$ are given by

$$\boldsymbol{u}(z) = [\hat{\boldsymbol{p}}_{3+}e^{-iw_3(z+d)} + \hat{\boldsymbol{p}}_{3-}r_{32}e^{iw_3(z+d)}]e^{iw_3 d}, \quad (15)$$

$$\boldsymbol{v}(z) = [\hat{\boldsymbol{p}}_{3+}r_{31}e^{-iw_3 z} + \hat{\boldsymbol{p}}_{3-}e^{iw_3 z}]e^{iw_3 d}. \quad (16)$$

The fields described by (13) can be readily generalized to other polarization distributions. For instance, consider a more general polarization field, $\tilde{\boldsymbol{P}}(\kappa;z)\exp(i\kappa y)$, and the associated electric field, $\tilde{\boldsymbol{E}}(\kappa;z)\exp(i\kappa y)$. In this case, the coefficients $\tilde{\boldsymbol{E}}(\kappa;z)$ are obtained by taking a linear superposition of the fields in (13) over the region $0 < z < -d$, which yields

$$\tilde{\boldsymbol{E}}(\kappa;z) = \frac{i\tilde{\omega}^2 p(\kappa)}{2\varepsilon_0 w_3}\int_{-d}^{0}\tilde{\boldsymbol{P}}(\kappa;z_0)\cdot\mathsf{q}(z,z_0)dz_0 - \frac{1}{\varepsilon_0\varepsilon_3}\tilde{\boldsymbol{P}}(\kappa;z)\cdot\hat{\boldsymbol{z}}\hat{\boldsymbol{z}}. \quad (17)$$

This expression describes the field in the slab structure generated by an arbitrary source polarization field distribution with a well defined κ.

We use these results in our nonlinear propagation problem by now taking $\tilde{\boldsymbol{P}}(\kappa;z_0)$ to be the nonlinear polarization in the metal, which must be determined self-consistently. To obtain the electric field radiated by the nonlinear polarization into the SPP mode m, we approximate $p(\kappa) \approx \varrho_m(\kappa-\kappa_m)^{-1}$, which is valid for values of κ close to κ_m (see Appendix A for details), and replace q by q^m and w_3 by w_3^m, where the superscript m has the usual meaning. After some algebra, one obtains

$$(\kappa-\kappa_m)\tilde{\boldsymbol{E}}(\kappa;z) = \eta(\kappa)\mathbf{e}(z) - \frac{(\kappa-\kappa_m)}{\varepsilon_0\varepsilon_3}\tilde{\boldsymbol{P}}(\kappa;z)\cdot\hat{\boldsymbol{z}}\hat{\boldsymbol{z}}, \quad (18)$$

where we have defined

$$\eta(\kappa) = \frac{i\tilde{\omega}^2\varrho_m}{2\varepsilon_0 w_3^m}t_{31}^m\int_{-d}^{0}\tilde{\boldsymbol{P}}(\kappa;z_0)\cdot\boldsymbol{u}^m(z_0)dz_0. \quad (19)$$

Note that the second term on the right-hand side of (18) is not part of the SPP field, but it results from the local contribution of the polarization. This term, however, is negligible when working with field intensities in the order of those required for a valid perturbative description of the nonlinear susceptibilities (see Appendix B for details). Thus we can write (18) as

$$(\kappa-\kappa_m)\tilde{\boldsymbol{E}}(\kappa;z) = \eta(\kappa)\mathbf{e}(z), \quad (20)$$

which describes the field radiated into the SPP modes of the slab ($m = \{s,a\}$) by the nonlinear polarization.

With this result, we proceed to obtain a differential equation to describe the evolution of $f(y)$ in the nonlinear regime. We start by noting that Eq. (20) holds when κ is sufficiently close to κ_m so that only the SPP excitation is important. With this in mind, we allow ourselves to write a more general field of the form

$$\boldsymbol{E}(\boldsymbol{r}) = \int\frac{d\kappa}{2\pi}\tilde{\boldsymbol{E}}(\kappa;z)e^{i\kappa y}, \quad (21)$$

where we allow κ to take only values close to κ_m'. Naturally, this field must have the form of that in (1), implying that the Fourier coefficients in (21) are given by

$$\tilde{\boldsymbol{E}}(\kappa;z) = \tilde{f}(\kappa-\kappa_m')\mathbf{e}(z), \quad (22)$$

where $\tilde{f}(\kappa)$ are the Fourier coefficients of $f(y)$; this is,

$$f(y) = \int\frac{d\kappa}{2\pi}\tilde{f}(\kappa)e^{i\kappa y}. \quad (23)$$

Here $f(y)$ not only describes the exponential decay of the field due to κ_m'', but also the nonlinear contribution from the field generated by the nonlinear polarization. Consequently, the differential equation describing the evolution of $f(y)$ is no longer homogeneous as in the linear case [i.e., Eq. (2)], but it must include an inhomogeneous term associated with the nonlinear polarization. To construct this differential equation, we first note from (22) and (20) that $(\kappa - i\kappa_m'')\tilde{f}(\kappa) = \eta(\kappa + \kappa_m')$. From this expression, we transform $\tilde{f}(\kappa)$ to the spatial domain using (23) and differentiate with respect to y to obtain

$$\frac{df(y)}{dy} = -\kappa_m'' f(y) + i\Lambda(y), \quad (24)$$

where

$$\Lambda(y) = \frac{i\tilde{\omega}^2\varrho_m}{2\varepsilon_0 w_3^m}t_{31}^m e^{-i\kappa_m' y}\int_{-d}^{0}\boldsymbol{P}(\boldsymbol{r})\cdot\boldsymbol{u}^m(z)dz. \quad (25)$$

Clearly, the first term on the right-hand side of (24) gives the decay of the SPP envelope function due to the linear losses, while the second term allows the field envelope to be modified by $\boldsymbol{P}(\boldsymbol{r})$.

C. SPP self-phase-modulation: Metal slab

Equation (24) describes the evolution of the SPP field envelope in a rather general fashion, as $\boldsymbol{P}(\boldsymbol{r})$ can have an arbitrary distribution. Nonetheless, this expression can be readily adapted to model the self-interaction of SPPs through the nonlinear response of the metal, which leads to SPP self-phase-modulation. This phenomenon is characterized by the complex nonlinear parameter, γ_m, which is defined such that the real (imaginary) part of the product $\gamma_m s(y)$ gives the local rate of nonlinear phase (nonlinear attenuation) experienced by the SPP upon propagation.

Consider first the s and a modes supported by the slab structure depicted in Fig. 1(a). From (25) we note that if $\boldsymbol{P}(\boldsymbol{r})$ results from the nonlinear response of the metal to a SPP field, then the term $\Lambda(y)$ in (24) will describe the self-phase-modulation of the SPP. Thus, taking the nonlinear polarization in the metal as $3\varepsilon_0\chi^{(3)}|\boldsymbol{E}(\boldsymbol{r})|^2\boldsymbol{E}(\boldsymbol{r})$, one obtains the nonlinear polarization induced by the SPP field as

$$\boldsymbol{P}(\boldsymbol{r}) = 3\varepsilon_0\chi^{(3)}|f(y)|^2 f(y)|\mathbf{e}(z)|^2\mathbf{e}(z)e^{i\kappa_m' y}.$$

Using this expression together with (11) in (25) one can rewrite the field envelope evolution equation as

$$\frac{df(y)}{dy} = -f(y)\kappa_m'' + if(y)s(y)\gamma_m, \quad (26)$$

with the complex nonlinear parameter given by

$$\gamma_m = \frac{3i\tilde{\omega}^2\chi^{(3)}\varrho_m}{2\mathcal{K}_m w_3^m}t_{31}^m\int_{-d}^{0}|\mathbf{e}_3(z)|^2\mathbf{e}_3(z)\cdot\boldsymbol{u}^m(z)dz \quad (27)$$

for $m = \{s,a\}$. A more explicit form of (27) is given in Appendix C. Note that since the field is uniform only in the x direction, γ_m has units of inverse power (W^{-1}) rather than more conventional units of length per unit of power that arise

for plane-wave propagation, where the field is uniform in the two directions perpendicular to the direction of propagation.

D. SPP self-phase-modulation: Single interface

Consider now the single metal-dielectric interface configuration depicted in Fig. 1(b), which corresponds to the case of an infinitely thick slab ($d \to \infty$). In this limit, only the c mode is supported at the interface between media 1 and 3. In this case, the SPP excitation is associated with the pole of the Fresnel coefficients r_{31} and t_{31}, from which the SPP propagation constant is obtained as [6]

$$\kappa_c = \tilde{\omega}\left(\frac{\varepsilon_1\varepsilon_3}{\varepsilon_1+\varepsilon_3}\right)^{1/2}. \tag{28}$$

By performing a Taylor expansion of the denominators of (5) about κ_c, we can express r_{31} and t_{31} for κ close to κ_c as

$$r_{31}^c \approx \frac{\rho_{31}}{\kappa-\kappa_c} \quad \text{with} \quad \rho_{31} = -\frac{2w_1^c\left(w_3^c\right)^2\varepsilon_1}{\kappa_c\left(w_3^c\varepsilon_3+w_1^c\varepsilon_1\right)}, \tag{29a}$$

$$t_{31}^c \approx \frac{\tau_{31}}{\kappa-\kappa_c} \quad \text{with} \quad \tau_{31} = -\frac{2\sqrt{\varepsilon_3}\sqrt{\varepsilon_1}w_1^c\left(w_3^c\right)^2}{\kappa_0\left(w_3^c\varepsilon_3+w_1^c\varepsilon_1\right)}. \tag{29b}$$

The results obtained in Sec. III C are simplified in the single interface limit for two reasons: (i) for $d \to \infty$ the poles and zeros of (7) cancel each other exactly [i.e., $p(\kappa) = 1$] leading to the expression $\varrho_c = \kappa - \kappa_c$; (ii) since there are no reflections from the bottom surface of the slab ($r_{32} = 0$), Eq. (15) becomes $\boldsymbol{u}^c(z) = \hat{\boldsymbol{p}}_{3+}^c \exp(-iw_3^c z)$ and the field in the metal becomes $\mathbf{e}_3^c(z) = r_{31}^c/t_{31}^c \exp(-iw_3^c z)\hat{\boldsymbol{p}}_{3-}^c$. Using these simplifications in (27), one finds

$$\gamma_c = \frac{3i\tilde{\omega}^2\chi^{(3)}}{2\mathcal{K}_c w_3^c}\tau_{31}\hat{\boldsymbol{p}}_{3+}^c\int_{-\infty}^{0}|\mathbf{e}_3^c(z)|^2\mathbf{e}_3^c(z)e^{-iw_3^c z}dz, \tag{30}$$

where we have used also (29b), and

$$\mathcal{K}_c = \frac{\mathrm{Re}(\kappa_c)}{\omega\mu_0}\left\{\frac{\mathrm{Re}(|\varepsilon_1|/\varepsilon_1)}{\mathrm{Im}(w_1^c)}+\left|\frac{\rho_{31}}{\tau_{31}}\right|^2\frac{\mathrm{Re}(|\varepsilon_3|/\varepsilon_3)}{\mathrm{Im}(w_3^c)}\right\}$$

has been obtained from (12) by setting $d \to \infty$ and noting that r_{31}^c diverges. Equation (30) can be integrated straightforwardly, and the result is given in Appendix C.

IV. RESULTS AND DISCUSSION

A. Complex nonlinear parameter of the SPP

We now apply the theory developed above to calculate the wavelength-dependent nonlinear parameters of the various SPP modes supported by the structures in Figs. 1(a) and 1(b). In particular, we consider as examples a 16-nm-thick Au slab surrounded by vacuum and a Au-vacuum interface. For these calculations we take $\varepsilon_1 = \varepsilon_2 = 1$ and assign to ε_3 the measured wavelength-dependent permittivity of Au reported in Palik's compendium [33]. Furthermore, we use the wavelength-dependent values of $\chi^{(3)}$ for Au shown in Fig. 2, which are obtained following the work of Marini *et al.* [25] assuming a continuous-wave excitation.

The calculated nonlinear parameters are shown in Fig. 3 over three different wavelength ranges. We follow the notation

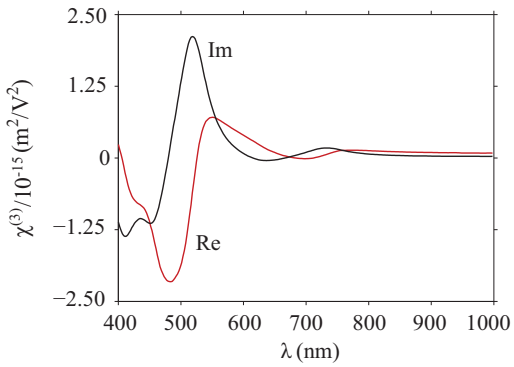

FIG. 2. (Color online) Complex $\chi^{(3)}$ values of Au as a function of the wavelength obtained following Marini *et al.* [25].

given above, with γ_s, γ_a, and γ_c denoting the nonlinear parameters of the s, a, and c modes, respectively. Moreover, we use γ_m to refer to them collectively. In the figures, the values of γ_s and γ_c have been multiplied by a factor of 10^6 and 400, respectively, before plotting.

The fact that γ_a is about one million times larger than γ_s and 400 times larger than γ_c is a manifestation of the different strengths with which these SPPs interact with the metal. Indeed, for the 16-nm-thick slab structure, the a mode is tightly confined to the metal slab having a very large portion of the electric field in the metal, while for the s mode the electric field is mostly localized in the vacuum region. For the c mode, on the other hand, the portion of the electric field localized in the metal is always larger (smaller) than that of the s mode (a mode). More generally, we found that the inequalities $\mathrm{Re}\gamma_a > \mathrm{Re}\gamma_c > \mathrm{Re}\gamma_s$ and $\mathrm{Im}\gamma_a > \mathrm{Im}\gamma_c > \mathrm{Im}\gamma_s$ always hold regardless of the slab's thickness. The exact values of γ_s and γ_a vary with the metal thickness, both approaching to the value of γ_c as the metal thickness increases (data not shown).

The values of γ_m in the range $760 < \lambda < 1000$ nm [Fig. 3(c)] have positive real and imaginary parts, implying an increment in the absorption and phase accumulation with increasing mode power. Also, in this wavelength range we observe an exponential increment of γ_m as the wavelength decreases. This feature results mainly from the stronger interaction of the SPP fields with the metal at the shorter wavelengths. Note from Fig. 2 that $\chi^{(3)}$ is practically constant over this wavelength range. Thus the rapid increment of γ_m is not related to the dispersion of $\chi^{(3)}$, but rather due to the linear dispersion of the SPP. On the other hand, γ_m exhibits an interesting behavior for $\lambda < 760$ nm partly because of the strong dispersion of $\chi^{(3)}$ in this region of the spectrum. For example, consider the wavelength range $620 < \lambda < 760$ nm [Fig. 3(b)]. Here we observe that both the real and the imaginary parts of γ_m exhibit decreasing and increasing trends, and over certain regions of the spectrum and that their values can be negative over certain regions of the spectrum. In particular, note that γ_m exhibits a negative imaginary part over the range $630 < \lambda < 670$ nm, indicating that for these wavelengths the SPP propagation loss is reduced as the mode power is increased. Finally, for wavelengths in the range $550 < \lambda < 620$ nm [Fig. 3(a)], both the real and imaginary parts of γ_m increase dramatically as the wavelength

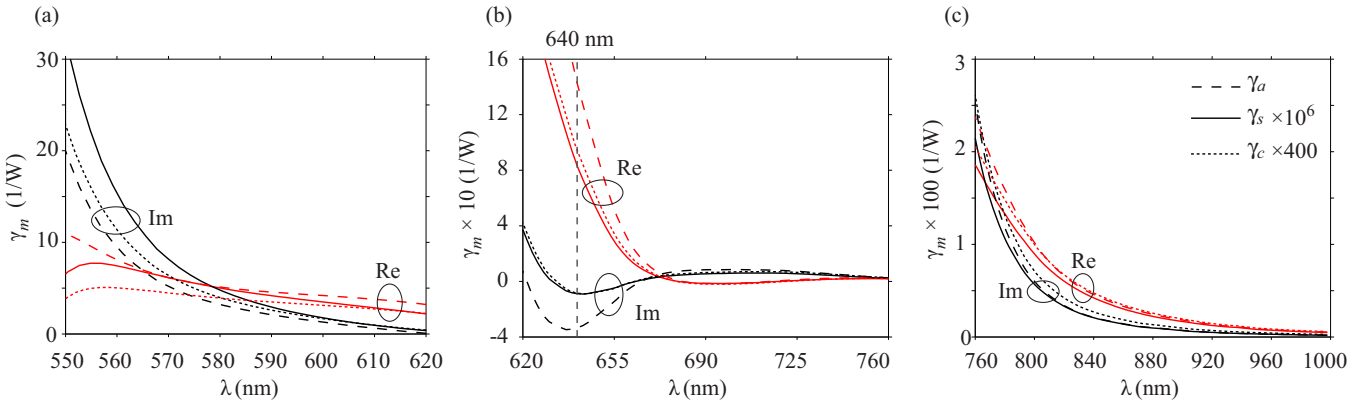

FIG. 3. (Color online) Complex nonlinear parameter of the various SPP modes $m = \{s,a,c\}$, calculated over three different wavelength ranges. The values of γ_s and γ_c have been multiplied by a factor of 10^6 and 400, respectively, before plotting.

is reduced. In this region of the spectrum, $\chi^{(3)}$ exhibits a strong dispersion caused by the interband electron transition from the d band to the sp band. Thus the effect observed is caused by both the large increment in the value of $\chi^{(3)}$ and the stronger field confinement in the metal that occurs over this wavelength range.

It is important to mention that the accuracy of these results is limited by the main approximation used in our theory; i.e., Eqs. (8) and (29). These approximations are accurate when the poles of the reflection (or transmission) coefficient are located close to the real axis in the complex κ plane (see Appendix A for details). As a result, the theory is not accurate when the imaginary part of κ_m is too large, or equivalently, when the propagation loss of the SPP is too large. Since the SPP propagation loss increases as the optical wavelength decreases [30,31], there exists a short-wavelength limit for the validity of our approximations. By comparing the exact reflection coefficients and their respective approximated forms, we found that Eqs. (8) and (29) are accurate to within 5% over the range $\lambda > 550$ nm for the s mode and c mode, and over the range $\lambda > 640$ nm for the a mode.

Also note that there is evidence indicating that the inferred value of $\chi^{(3)}$ for metals like Au depends strongly upon the laser pulse duration that is used [25,34]. Thus the values of γ_m reported in Fig. 3 may not represent faithfully those obtained in experiments using ultrashort pulses.

B. Nonlinear phase shift and attenuation

Knowing γ_m, one can estimate the strength of the self-phase-modulation for given launching power $s_0 \equiv s(y = y_0)$ by solving for $f(y)$ in Eq. (24). Without loss of generality, we assume that the SPP is launched at the position $y_0 = 0$ and calculate the SPP position-dependent nonlinear phase shift and the total power attenuation (linear and nonlinear contributions) as

$$\phi_{\mathrm{NL}}(y) = \tan^{-1}\left[\frac{\mathrm{Im}\, f(y)}{\mathrm{Re}\, f(y)}\right], \quad A(y) = \left|\frac{f(y)}{f(0)}\right|^2,$$

respectively. The maximum nonlinear phase shift acquired by the SPP is thus given by $\bar{\phi}_{\mathrm{NL}} = \phi_{\mathrm{NL}}(\ell_{\mathrm{SP}})$, where ℓ_{SP} is the SPP propagation length, defined as the distance y at which $A(y) = \exp(-1)$.

As an example, we consider the structures studied above operating at the wavelength $\lambda = 640$ nm. Note from Fig. 3(b) that $\mathrm{Im}\gamma_m < 0$ at this wavelength, indicating SPP propagation loss reduction with increasing power. In our calculations we set the value of s_0 such that the ratio of nonlinear polarization to linear polarization is ∼0.1, which ensures compliance with the perturbative approximation for the nonlinear polarization made in our analysis [i.e., Eq. (B3)]. Table I tabulates $\bar{\phi}_{\mathrm{NL}}$ and ℓ_{SP} obtained for the various SPP modes by solving Eq. (24) using the adaptive Runge-Kutta method. The values of γ_m and s_0 used for each calculation are also given in the table.

The values of $\bar{\phi}_{\mathrm{NL}}$ are comparable for the three modes because the product $\mathrm{Re}\gamma_m s_0 \ell_{\mathrm{SP}}$ turns out to be very similar for the three cases. Furthermore, despite the large values of γ_m, the parameter $\bar{\phi}_{\mathrm{NL}}$ is always small because ℓ_{SP} is very short. We note that the short propagation lengths are mainly dictated by the linear losses. Indeed, the loss reduction resulting from the nonlinearity was calculated as ∼10% for all the modes. In practice, one could use a larger launching power, s_0, to obtain a larger $\bar{\phi}_{\mathrm{NL}}$ as long as structural damage does not occur. However, to accurately model self-phase-modulation using values of s_0 larger than those used here, it would be necessary to employ a nonperturbative nonlinear polarization model.

While the values of $\bar{\phi}_{\mathrm{NL}}$ obtained here are small, the corresponding nonlinear phase shifts per unit length (i.e., $\bar{\phi}_{\mathrm{NL}}/\ell_{\mathrm{SP}}$) are very large. For instance, for the a and c modes, this figure is equivalent to acquiring a nonlinear phase shift of π radians in a lossless system over a distance of only ∼4 μm and ∼73 μm, respectively. Clearly, extending the propagation length of these SPPs could increase significantly the acquired

TABLE I. Self-phase-modulation parameters of the various SPP modes at $\lambda = 640$ nm.

m	s	a	c
$\mathrm{Re}\gamma_m$ (W^{-1})	8.29×10^{-7}	1.42	2.27×10^{-3}
$\mathrm{Im}\gamma_m$ (W^{-1})	-0.88×10^{-7}	−0.33	-0.21×10^{-3}
s_0 (kW/mm)	1130	0.83	30
$\bar{\phi}_{\mathrm{NL}}$ (rad)	$\pi/9.2$	$\pi/9.1$	$\pi/9.0$
ℓ_{SP} (μm)	568.6	0.455	7.47

nonlinear phase shift. Recently, optical amplification of SPP has been demonstrated in similar plasmonic structures [35]; thus increasing the SPP propagation length by this means could be a possible strategy to take advantage of the large nonlinear effect.

C. Comparison with an experimental result

The nonlinear response of the SPP supported by a Au film in the Kretschmann configuration was recently investigated by some of us [36] using a pulsed laser excitation with a pulse duration of ∼100 fs and a wavelength of 796 nm. The Kretschmann structure consisted of a 48-nm-thick Au film with one of its surfaces in direct contact with a glass substrate and the other bounded by air. In this experiment, the complex nonlinear parameter of the Kretschmann SPP was obtained as $\gamma_K = (8.08 + i1.46) \times 10^{-7}$ 1/W from measurements of the intensity-dependent attenuated total internal reflection. The experiment also allowed for the extraction of the nonlinear susceptibility of Au, which resulted in a value of $\chi^{(3)} = (4.67 + i3.03) \times 10^{-19}$ V^2/m^2. We note that this value of $\chi^{(3)}$ is about 100 times smaller than the theoretical estimation in Fig. 2 (for continuous-wave light), which is consistent with other experimental observations [34].

The Kretschmann SPP studied in Ref. [36] is similar to the c mode of the single Au-air interface structure. They both exhibit a very similar electromagnetic field profile in the metal and air regions. However, they differ in that the Kretschmann SPP extends part of its field into the glass substrate, making the mode leaky [6]. As a result, the propagation constant of the Kretschmann SPP is slightly different from that of the c mode. Nonetheless, the similarities between these two modes allows us to draw a fair comparison of their nonlinear responses.

Using the measured value of $\chi^{(3)}$ in (30), we obtain $\gamma_c = (1.03 + i0.98) \times 10^{-7}$ 1/W. This result agrees with the measured value of γ_K to within an order of magnitude. The discrepancy can be attributed in part to the approximations made in our theory and to the differences between the Kretschmann and c modes. Yet other reasons with deeper physical significance may exist. For instance, a contribution to the nonlinear response arising from the metal surface and finite thickness of the metal could exist in addition to the usual bulk contribution. Evidence of these contributions, which are not accounted for in the present theory, have been recently reported by other groups [37,38] in the context of SPP four-wave mixing and third-harmonic generation. However, these phenomena remain largely unexplored in the context of SPP self-phase-modulation. Thus more work is needed to understand the various mechanisms that can contribute to the nonlinear response of simple plasmonic structures such as the ones studied here, aiming to achieve a better understanding of the fundamental nonlinear interactions in more complex plasmonic structures.

V. SUMMARY AND CONCLUSIONS

In summary, we have presented an approach to model the intrinsic nonlinear response (i.e., that arising from the nonlinearity of the metal) of SPPs supported by two standard plasmonic waveguides: the metal slab and semi-infinite metal bounded by linear dielectrics. Our formulation employs a Green-function formalism to model the SPP fields resulting from an arbitrary nonlinear polarization in the metal. This approach was then used to study the case where SPPs interact with themselves through the third-order nonlinear response of the metal, leading to SPP self-phase-modulation. We provided equations that relate directly the SPP nonlinear propagation coefficient with the metal's $\chi^{(3)}$ coefficient. This relation has practical importance, as it allows one to estimate the complex value of $\chi^{(3)}$ of plasmonic materials through a measurement of SPP nonlinear propagation coefficient. Also, we presented and discussed numerical results for self-phase-modulation of the symmetric and antisymmetric SPP modes supported by a thin Au slab in vacuum, and of the SPP mode supported at a single Au-vacuum interface. We discussed aspects such as the substantial difference between the nonlinear parameter of these three modes and their strongly dispersive characteristics. Finally, we provided a comparison between the SPP nonlinear parameter estimated by our theory and that measured in a recent experiment.

ACKNOWLEDGMENTS

I.D.L. would like to thank Pierre Berini for valuable discussions. R.W.B. would like to thank Barry Sanders and Pierre Berini for useful discussions on the use of SPPs in the context of quantum information processing. J.E.S. would like to thank the Natural Sciences and Engineering Research Council of Canada (NSERC) for supporting this research. The work performed at the University of Ottawa was supported by the Canada Excellence Research Chairs (CERC) program.

APPENDIX A: EXPRESSING THE RESPONSE COEFFICIENTS USING A POLE EXPANSION OF $p(\kappa)$

Here we detail the steps taken to represent the response coefficients in (6) using a pole expansion of $p(\kappa)$. We start by using the expression for r_{ij} as given by (5) into (7) and write

$$p(\kappa) = \frac{a_1 a_2}{a_1 a_2 - b_1 b_2 e^{2iw_3 d}}, \tag{A1}$$

where $a_i = (w_i \varepsilon_3 + w_3 \varepsilon_i)$ and $b_i = (w_i \varepsilon_3 - w_3 \varepsilon_i)$. Here, the expression $a_1 a_2 - b_1 b_2 e^{2iw_3 d} = 0$ is the dispersion relation for the SPP modes supported by the slab and the solutions of this equation identify the poles of $p(\kappa)$. Similarly, the expressions $a_1 = 0$ and $a_2 = 0$ denote the dispersion relations of single-interface SPPs localized at the interface between media 1-3 and 2-3, respectively; the solutions to these equations identify the zeros of $p(\kappa)$. One can express (A1) as a rational function of poles and zeros [39],

$$p(\kappa) = \mathcal{A}(\kappa) \frac{Z(\kappa)}{P(\kappa)}, \tag{A2}$$

where $\mathcal{A}(\kappa)$ is a slowly varying function of κ, and

$$P(\kappa) = \prod_m (\kappa - \kappa_m), \quad Z(\kappa) = \prod_l (\kappa - \kappa_l),$$

are the pole and zero functions, with κ_m and κ_l being the complex propagation constants associated with the poles and

zeros of (A1), respectively. Expressing $P(\kappa)$ as a partial fraction expansion, we write (A2) as

$$p(\kappa) = \sum_m \frac{\varrho_m(\kappa)}{\kappa - \kappa_m}, \tag{A3}$$

where $\varrho_m(\kappa) = \mathcal{A}(\kappa)Z(\kappa)\mathrm{Res}[P(\kappa),\kappa_m]$ with the quantity $\mathrm{Res}[P(\kappa),\kappa_m]$ denoting the residue of $P(\kappa)$ at κ_m.

To derive (8), we assume that the poles are far from each other in the complex plane and sufficiently close to the real axis such that we can approximate (A3) for values of κ close to κ_m as the contribution of the one pole at κ_m,

$$p(\kappa) \approx \frac{\varrho_m}{\kappa - \kappa_m}, \tag{A4}$$

where we have defined $\varrho_m \equiv \varrho_m(\kappa'_m)$, since $\varrho_m(\kappa)$ varies slowly compared to $(\kappa - \kappa_m)^{-1}$ in the vicinity of κ_m. Finally, substituting (A4) in (6) yields (8).

APPENDIX B: APPLICABILITY OF EQ. (20)

Equation (20) is valid when the second term on the right-hand side of (18) is negligible. Here, we determine the situation under which such a condition is valid. We start by rewriting (18) as $(\kappa - \kappa_m)\tilde{\boldsymbol{G}}(\kappa;z) = \eta(\kappa)\mathbf{e}(z)$, where

$$\tilde{\boldsymbol{G}}(\kappa;z) = \tilde{\boldsymbol{E}}(\kappa;z) + \frac{1}{\varepsilon_0\varepsilon_3}\tilde{\boldsymbol{P}}(\kappa;z)\cdot\hat{z}\hat{z}, \tag{B1}$$

and using the relation $\tilde{\boldsymbol{P}}(\kappa;z) = 3\varepsilon_0\chi^{(3)}|\tilde{\boldsymbol{E}}(\kappa;z)|^2\tilde{\boldsymbol{E}}(\kappa;z)$ in the equation above, we write

$$\tilde{\boldsymbol{G}}(\kappa;z)\cdot\hat{z} = \left(1 + \frac{3\chi^{(3)}}{\varepsilon_3}|\tilde{\boldsymbol{E}}(\kappa;z)|^2\right)\tilde{\boldsymbol{E}}(\kappa;z)\cdot\hat{z}. \tag{B2}$$

Since $\tilde{\boldsymbol{G}}(\kappa;z)$ and $\tilde{\boldsymbol{E}}(\kappa;z)$ only differ in their z components, it is clear from this result that one can approximate $\tilde{\boldsymbol{G}}(\kappa;z) \approx \tilde{\boldsymbol{E}}(\kappa;z)$ when

$$|\chi^{(1)}| \gg 3|\chi^{(3)}||\tilde{\boldsymbol{E}}(\kappa;z)|^2, \tag{B3}$$

where we have used $|\varepsilon_3| = |\chi^{(1)} + 1| \approx |\chi^{(1)}|$. Another important inequality that must be satisfied in the nonlinear regime is

$$|\chi^{(1)}| \gg |\chi^{(3)}||\tilde{\boldsymbol{E}}(\kappa;z)|^2, \tag{B4}$$

which is required for the usual expansion of the total polarization [29] to make physical sense. Note that the right-hand side of (B3) is only three times larger that the right-hand side of (B4). Thus both inequalities are satisfied with fields $|\tilde{\boldsymbol{E}}(\kappa;z)|^2$ of the same order of magnitude. In our calculations we restrict ourselves to consider fields that satisfy (B3), and hence also satisfy (B4).

APPENDIX C: EXPLICIT EXPRESSION FOR THE SPP NONLINEAR PROPAGATION COEFFICIENT

An expression for the nonlinear parameter of the SPP modes of the slab was given in (27) in terms of the transverse SPP field distribution, $\mathbf{e}(z)$, and the function $\boldsymbol{u}^m(z)$. Here, we further develop these results and provide a more explicit form for this expression. We start by noting that for the SPP modes of the slab, $m = \{s,a\}$, we can use the dispersion relation $r^m_{31}r^m_{32}\exp(2iw^m_3 d) = 1$ and write

$$\mathbf{e}_3(z) = \frac{1}{t^m_{31}}\left(\hat{\boldsymbol{p}}^m_{3+}\frac{1}{g_m} + \hat{\boldsymbol{p}}^m_{3-}r^m_{31}g_m\right),$$

$$\boldsymbol{u}^m(z) = \hat{\boldsymbol{p}}^m_{3+}g_m + \hat{\boldsymbol{p}}^m_{3-}\frac{1}{r^m_{31}g_m},$$

where we have defined $g_m \equiv \exp(-iw^m_3 z)$. Then using these expressions in (27) one finds

$$\gamma_m = \frac{3i\tilde{\omega}^2\chi^{(3)}\varrho_m}{2\mathcal{K}_m w^m_3}\left|\frac{r^m_{31}}{t^m_{31}}\right|^2 r^m_{31}\mathcal{I}_m \tag{C1}$$

for $m = \{s,a\}$, where

$$\mathcal{I}_m = \int_{-d}^{0} dz\left[Q_1|g_m|^2 + \frac{Q_1}{|r^m_{31}g_m|^2} + \frac{2Q_2}{r^m_{31}}\cos\left(2w^m_3 z\right)\right]$$
$$\times\left[Q_3(g_m)^2 + \frac{Q_3}{\left(r^m_{31}g_m\right)^2} + \frac{2Q_4}{r^m_{31}}\right] \tag{C2}$$

and the following shorthand notation has been used:

$$Q_1 = \hat{\boldsymbol{p}}^m_{3+}\cdot\hat{\boldsymbol{p}}^{m*}_{3+} = \hat{\boldsymbol{p}}^m_{3-}\cdot\hat{\boldsymbol{p}}^{m*}_{3-},$$
$$Q_2 = \hat{\boldsymbol{p}}^m_{3+}\cdot\hat{\boldsymbol{p}}^{m*}_{3-} = \hat{\boldsymbol{p}}^m_{3-}\cdot\hat{\boldsymbol{p}}^{m*}_{3+},$$
$$Q_3 = \hat{\boldsymbol{p}}^m_{3+}\cdot\hat{\boldsymbol{p}}^{m}_{3-} = \hat{\boldsymbol{p}}^m_{3-}\cdot\hat{\boldsymbol{p}}^{m}_{3+},$$
$$Q_4 = \hat{\boldsymbol{p}}^m_{3+}\cdot\hat{\boldsymbol{p}}^{m}_{3+} = \hat{\boldsymbol{p}}^m_{3-}\cdot\hat{\boldsymbol{p}}^{m}_{3-}.$$

As discussed in Sec. III D, for $d \to \infty$ we have $r^c_{31} \to \infty$ and $\varrho_c = \kappa - \kappa_c$. Thus, for the c mode supported by the single-interface structure, (C1) becomes

$$\gamma_c = \frac{3i\tilde{\omega}^2\chi^{(3)}}{2\mathcal{K}_c w^c_3}\left|\frac{\rho_{31}}{\tau_{31}}\right|^2\rho_{31}\mathcal{I}_c, \tag{C3}$$

where ρ_{31} and τ_{31} are defined in (29) and

$$\mathcal{I}_c = \int_{-\infty}^{0} dz\, Q_1 Q_3 |g_c|^2 (g_c)^2 = \frac{Q_1 Q_3}{2\left(\mathrm{Im}w^c_3 - iw^c_3\right)}. \tag{C4}$$

[1] Y. Wang, C.-Y. Lin, A. Nikolaenko, V. Raghunathan, and E. O. Potma, Adv. Opt. Photon. **3**, 1 (2011).

[2] G. Cerullo and S. De Silvestri, Rev. Sci. Instrum. **74**, 1 (2003).

[3] M. Fejer, Phys. Today **47**, 25 (1994).

[4] D. Cotter, R. Manning, K. Blow, A. Ellis, and A. Kelly, Science **286**, 1523 (1999).

[5] M. Kauranen and A. V. Zayats, Nat. Photon. **6**, 737 (2012).

[6] H. Raether, *Surface Plasmons on Smooth and Rough Surfaces and on Gratings* (Springer, Berlin, 1988).

[7] W. L. Barnes, A. Dereux, and T. W. Ebbesen, Nature (London) **424**, 824 (2003).

[8] J. A. Schuller, E. S. Barnard, W. Cai, Y. C. Jun, J. S. White, and M. L. Brongersma, Nat. Mater. **9**, 193 (2010).

[9] T. Y. F. Tsang, Opt. Lett. **21**, 245 (1996).

[10] P. Wang, Y. Lu, L. Tang, J. Zhang, H. Ming, J. Xie, F. Ho, H. Chang, H. Lin, and D. Tsai, Opt. Commun. **229**, 425 (2004).
[11] J. Renger, R. Quidant, N. van Hulst, and L. Novotny, Phys. Rev. Lett. **104**, 046803 (2010).
[12] P. Genevet, J.-P. Tetienne, E. Gatzogiannis, R. Blanchard, M. A. Kats, M. O. Scully, and F. Capasso, Nano Lett. **10**, 4880 (2010).
[13] R. J. Gehr, G. L. Fischer, R. W. Boyd, and J. E. Sipe, Phys. Rev. A **53**, 2792 (1996).
[14] N. N. Lepeshkin, A. Schweinsberg, G. Piredda, R. S. Bennink, and R. W. Boyd, Phys. Rev. Lett. **93**, 123902 (2004).
[15] T. Utikal, M. I. Stockman, A. P. Heberle, M. Lippitz, and H. Giessen, Phys. Rev. Lett. **104**, 113903 (2010).
[16] F. Hache, D. Ricard, and C. Flytzanis, J. Opt. Soc. Am. B **3**, 1647 (1986).
[17] H. Wang, T. B. Huff, D. A. Zweifel, W. He, P. S. Low, A. Wei, J.-X. Cheng, and Y. R. Shen, Proc. Natl. Acad. Sci. USA **102**, 15752 (2005).
[18] M. Lippitz, M. A. van Dijk, and M. Orrit, Nano Lett. **5**, 799 (2005).
[19] A. Bouhelier, R. Bachelot, G. Lerondel, S. Kostcheev, P. Royer, and G. P. Wiederrecht, Phys. Rev. Lett. **95**, 267405 (2005).
[20] D. Mihalache, G. I. Stegeman, C. T. Seaton, E. M. Wright, R. Zanoni, A. D. Boardman, and T. Twardowski, Opt. Lett. **12**, 187 (1987).
[21] H. Yin, C. Xu, and P. M. Hui, Appl. Phys. Lett. **94**, 221102 (2009).
[22] J.-H. Huang, R. Chang, P.-T. Leung, and D. P. Tsai, Opt. Commun. **282**, 1412 (2009).
[23] A. R. Davoyan, I. V. Shadrivov, and Y. S. Kivshar, Opt. Express **16**, 21209 (2008).
[24] A. Degiron and D. R. Smith, Phys. Rev. A **82**, 033812 (2010).
[25] A. Marini, M. Conforti, G. D. Valle, H. W. Lee, W. C. Tr. X. Tran, M. A. Schmidt, S. Longhi, P. S. J. Russell, and F. Biancalana, New J. Phys. **15**, 013033 (2013).
[26] Y. Liu, G. Bartal, D. A. Genov, and X. Zhang, Phys. Rev. Lett. **99**, 153901 (2007).
[27] E. Feigenbaum and M. Orenstein, Opt. Lett. **32**, 674 (2007).
[28] F. Hache, D. Ricard, C. Flytzanis, and U. Kreibig, Appl. Phys. A **47**, 347 (1988).
[29] R. W. Boyd, *Nonlinear Optics*, 3rd ed. (Academic Press, New York, 2008).
[30] E. N. Economou, Phys. Rev. **182**, 539 (1969).
[31] J. J. Burke, G. I. Stegeman, and T. Tamir, Phys. Rev. B **33**, 5186 (1986).
[32] J. E. Sipe, J. Opt. Soc. Am. B **4**, 481 (1987).
[33] E. D. Palik, *Handbook of Optical Constants of Solids* (Academic Press, New York, 1985).
[34] N. Rotenberg, A. D. Bristow, M. Pfeiffer, M. Betz, and H. M. van Driel, Phys. Rev. B **75**, 155426 (2007).
[35] P. Berini and I. De Leon, Nat. Photon. **6**, 16 (2011).
[36] I. De Leon, Z. Shi, A. C. Liapis, and R. W. Boyd (unpublished).
[37] S. Palomba and L. Novotny, Phys. Rev. Lett. **101**, 056802 (2008).
[38] S. V. Fomichev, S. V. Popruzhenko, D. F. Zaretsky, and W. Becker, J. Phys. B: At. Mol. Opt. Phys. **36**, 3817 (2003).
[39] E. Anemogiannis, E. N. Glytsis, and T. K. Gaylord, J. Lightwave Technol. **17**, 929 (1999).